ACS OMEGA

Open Access

http://pubs.acs.org/journal/acsodf

Article

Effect of Acid–Base Property on the Upgrade of Ethanol and Acetaldehyde to Butadiene over Sc_2O_3–SiO_2 Catalysts

Qiangqiang Zhu, Lilin Yin, Xianyao Han, and Bin Wang*

Cite This: *ACS Omega* 2025, 10, 7069–7076

Read Online

ACCESS | Metrics & More | Article Recommendations | Supporting Information

ABSTRACT: A novel Sc_2O_3–SiO_2 catalyst was explored and evaluated for the upgrade of ethanol and acetaldehyde to butadiene. Notably, the Sc_2O_3–SiO_2 catalyst with a Sc/Si molar ratio of 0.06 demonstrated exceptional performance, exhibiting the highest selectivity of 81.7% for butadiene alongside a selectivity of 10.2% for butanol. When the Sc/Si ratio was increased to 0.3, the butanol selectivity increased to 30.0%. To elucidate the underlying factors governing these results, detailed characterizations of the catalysts structure and acidic–basic properties were conducted for the Sc_2O_3–SiO_2 materials. The analyses revealed that the higher percentage of strong acidic sites in total acidic sites was conducive to higher butadiene yield, while the increased density of strong basic sites correlated with higher butanol selectivity.

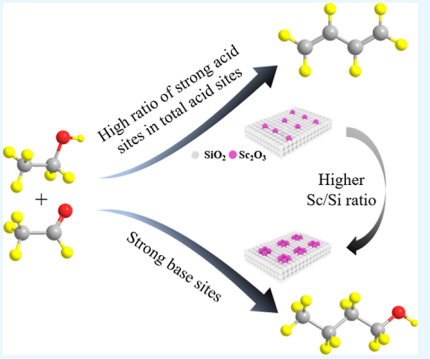

1. INTRODUCTION

Butadiene, a vital asymmetric synthetic intermediate, serves as the foundation for synthesizing a plethora of polymers, including synthetic rubber, plastics, and polyamides.[1−3] With a global annual demand reaching 14.2 million tons in recent years,[4] butadiene plays a pivotal role in various industrial applications. Traditionally, butadiene is primarily obtained as a byproduct in the naphtha cracking process of the petrochemical industry, with over 91% of the world's supply.[5] However, the decline in naphtha cracking due to the widespread extraction of shale gas has led to reduced butadiene production and escalated prices.[6] Consequently, there is a pressing need to explore alternative production routes. Recently, there has been a growing emphasis on the utilization of renewable natural resources to address sustainability concerns. The upgrade of ethanol (EtOH) to butadiene emerges as a promising alternative, tapping into biomass-derived sources for butadiene synthesis.

The direct upgrade of EtOH to butadiene involves a highly complex tandem reaction. Scheme 1 outlines the generally accepted mechanism for converting EtOH to butadiene:[7−10] (1) dehydrogenation of EtOH to acetaldehyde (AA), (2) condensation of two molecules of AA to form acetaldol via aldol condensation, (3) acetaldol dehydration to crotonaldehyde, (4) upgrade of crotonaldehyde to crotyl alcohol through the Meerwein–Ponndorf–Verley (MPV) reduction, and (5) crotyl alcohol dehydration to butadiene.

Various catalyst systems have been developed for the conversion of EtOH to butadiene. These include MgO–SiO_2,[7,10−12] ZrO_2–SiO_2,[13−16] HfO_2–SiO_2,[17−19] and Y_2O_3–SiO_2,[20,21] as well as Ta_2O_5–SiO_2-based catalysts[22−24], which have been thoroughly investigated and shown to exhibit high catalytic performances. Additionally, it has been widely reported that Ag, Cu, and Zn can be added to two-component catalysts to prepare three-component catalysts.[8,23,25] The presence of Ag and Zn enhances the conversion of EtOH to AA, while Mg, Zr, and Ta primarily enhance the upgrade of EtOH-AA to butadiene.

Scheme 1. Mechanism of EtOH-to-Butadiene Conversion

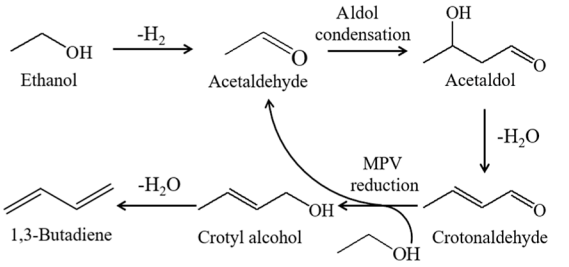

Therefore, efficient production of butadiene from EtOH can be achieved through either a one-step process using M_1–M_2O_x–SiO_2 catalysts (where M_1 represents Ag, Cu, and Zn, and M_2O_x represents MgO, ZrO_2, Ta_2O_5, HfO_2, and Y_2O_3)[15,16,20,26] or a two-step process using M_1–SiO_2 (where M_1 represents Ag, Cu, and Zn) and M_2O_x–SiO_2 catalysts

Received: November 7, 2024
Revised: February 5, 2025
Accepted: February 7, 2025
Published: February 17, 2025

https://doi.org/10.1021/acsomega.4c10129
ACS Omega 2025, 10, 7069–7076

(where M_2O_x represents MgO, ZrO_2, Ta_2O_5, and Y_2O_3).[10,27−29] In the two-step process, EtOH is first partially dehydrogenated to AA over the M_1−SiO_2 catalysts, and then EtOH-AA is transformed into butadiene over the M_2O_x−SiO_2 catalysts as the second step. Considering that EtOH can be synthesized into AA with a selectivity of over 98%,[30] the key to achieving high selectivity in the EtOH upgrade to butadiene lies in the development of highly selective catalysts for the EtOH-AA upgrade into butadiene. Additionally, understanding the underlying factors in the EtOH-AA upgrade to butadiene, such as acidic−basic properties, is of significance to enhancing butadiene selectivity.

In this work, we explore the catalytic activity of a novel Sc_2O_3−SiO_2 catalyst for butadiene production from EtOH-AA. Initially, we investigate the impact of the reaction parameters and Sc/Si ratio on the catalytic activity. A high butadiene selectivity of 81.7% was achieved, while the total selectivity of butadiene and butanol exceeded 90%. Subsequently, to elucidate the relationship between catalyst properties and performance, the Sc_2O_3−SiO_2 materials with varying Sc/Si ratios were prepared and characterized using various techniques. The effect of acidic and basic properties on the formation of butadiene and butanol was revealed.

2. EXPERIMENTAL SECTION

2.1. Materials and Chemicals. EtOH (HPLC, Fisher chemical), AA (99.5%, Adamas Reagent Co.), scandium chloride hexahydrate ($ScCl_3{\cdot}6H_2O$, 99.99%, Sigma-Aldrich), scandium oxide (99.99%, metals basis, Sigma-Aldrich), and fumed silica (SiO_2, WACKER HDK) were all used as received without further purification. EtOH-AA is a mixture of EtOH and AA, which are manually mixed in a weight ratio of 3:1.

2.2. Catalyst Preparation. The Sc_2O_3−SiO_2 materials with varying Sc/Si molar ratios were prepared by using the impregnation method with water as the solvent. The preparation of the Sc_2O_3−SiO_2 material with a Sc/Si molar ratio of 0.06 is presented as a typical example. 1.297 g of $ScCl_3{\cdot}6H_2O$ was dissolved in 50 g of water at 30 °C. Subsequently, 5.0 g of SiO_2 was slowly introduced to the obtained solution under constant stirring. The resulting suspension was stirred continuously at 80 °C until complete evaporation of water occurred. Finally, the obtained composition was calcined at 500 °C for 3 h with a heating rate of 5 °C/min. The same procedure was employed to prepare other catalysts.

2.3. Catalyst Characterization. Nitrogen (N_2) adsorption and desorption tests were performed by using a Micromeritics ASAP 2020 HD 88 surface area and porosity analyzer. Prior to these analyses, each sample underwent a pretreatment process at 180 °C under vacuum for 10 h.

X-ray diffraction (XRD) measurements were conducted by utilizing a Bruker diffractometer equipped with Cu radiation (40 kV, 120 mA). Data acquisition was performed within the 2θ range of 5−90°, employing an angular step size of 0.2°.

The acidic and basic properties of the catalysts were assessed by using temperature-programmed desorption (TPD) with a TCD detector. For each TPD measurement, 0.1 g of catalyst was employed. The sample underwent pretreatment in a quartz U-tube at 450 °C for 45 min under helium flow. Then, the sample was cooled to 80 °C, and the probe gas (NH_3 or CO_2) was introduced into the quartz U-tube for 30 min. After eliminating the physisorbed probe gas by evacuating the catalyst at the same temperature (80 °C) for 45 min, the temperature was ramped from 80 to 500 °C at a rate of 10 °C/min under a helium flow of 20 mL/min. Both the temperature and TCD signals were recorded from 80 to 500 °C.

2.4. Catalytic Performance Evaluation. The upgrade of EtOH-AA (75:25 wt %) to butadiene was conducted in a fixed bed with a quartz reactor of 8 mm internal diameter under atmospheric pressure (1 bar). The entire catalyst evaluation system design is shown in Figure 1. It includes a feed pump,

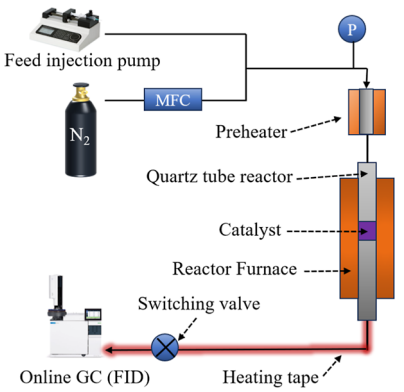

Figure 1. Schematic diagram of the catalytic reaction setup. MFC: mass flow controller; P: pressure gauge.

carrier gas tank, preheating system, reaction system, and online Gas Chromatography (GC) detection system. The reactor is a transparent hollow quartz tube prepared by Beijing KaiDe Quartz Co., Ltd. with a length of 300 mm, an inner diameter of 8 mm, and an outer diameter of 10 mm. Additionally, the quartz tube is connected to the pipelines using polytetrafluoroethylene ferrules. Helium was used as the carrier gas with a flow rate of 6 mL min^{-1}. Typically, the catalyst (0.6 g) was first loaded into the quartz reactor and heated to the reaction temperature under nitrogen flow at 5 °C min^{-1}. Then the EtOH-AA mixture with a flow rate of 0.36 mL h^{-1} (0.28 g h^{-1}) was introduced into the reactor using a Longer injection pump (LSP01-3A) purchased from Halma International Ltd. The evaluation proceeded for 4 h in a continuous flow. The output was kept at 180 °C and analyzed online through a Shimadzu GC instrument equipped with a flame ionization detector and an HP-PLOT-Q column. This setup could detect various products, including ethylene, propylene, butadiene, butylene isomers, diethyl ether, and C_4 compounds.

The conversion of EtOH-AA, the selectivity of products (S_i), carbon balance, and weight hourly space velocity (WHSV) are calculated using the following equations

$$\text{EtOH-AA conversion (\%)} = \frac{(n_{\text{EtOH}} + n_{\text{AA}}) - (n_{\text{unreactedEtOH}} + n_{\text{unreactedAA}})}{(n_{\text{EtOH}} + n_{\text{AA}})} \times 100\% \quad (1)$$

$$S_i\ (\%) = \frac{n_i}{(n_{\text{EtOH}} + n_{\text{AA}}) - (n_{\text{unreactedEtOH}} + n_{\text{unreactedAA}})} \times 100\% \quad (2)$$

$$\text{Carbon balance (\%)} = \sum S_i \quad (3)$$

$$\text{WHSV (g g}^{-1}\text{ h}^{-1}) = \frac{m_{\text{EtOH}} + m_{\text{AA}}}{m_{\text{catalyst}} \times t} \quad (4)$$

https://doi.org/10.1021/acsomega.4c10129
ACS Omega 2025, 10, 7069−7076

where i includes ethylene, propylene, butadiene, butylene isomers, diethyl ether, and C_4 compounds; n_i presents the amount of C moles of product i; m presents the mass of catalyst or feed; and t presents reaction time.

3. RESULTS AND DISCUSSION

3.1. Influence of Sc/Si Ratio on Catalytic Activity for the Sc_2O_3−SiO_2 Materials. Figure 2 and Table 1 exhibit the influence of the Sc/Si molar ratio on catalytic activity for the Sc_2O_3−SiO_2 materials. The conversion of EtOH-AA and the selectivity of butadiene present a volcanic curve with the Sc/Si ratio rising from 0.01 to 0.3. The best conversion of EtOH-AA (28.7%) and selectivity of butadiene (81.7%) were obtained when the Sc/Si ratio is 0.06. An enhanced Sc/Si ratio leads to an obvious change in the product distribution. With increasing Sc/Si ratio, the total selectivities of ethylene and diethyl ether continuously decrease from 17.1% to 3.4%, while butanol selectivity distinctly increases from 1.6% to 29.1%. The Sc/Si ratio of 0.3 provides a high selectivity of butanol up to 30.0%. The blank (no catalyst) and the SiO_2 support were also performed under the same experimental conditions as the Sc_2O_3−SiO_2 catalysts. In the absence of any catalyst, the conversion rate was less than 1%. When SiO_2 was used as the catalyst, the conversion rate increased to 3.5%, with a selectivity of 88.1% toward crotonaldehyde and 11.9% selectivity toward butanol. These results highlight that the bare SiO_2 support itself has limited catalytic activity but does contribute to some conversion. More importantly, the role of Sc_2O_3 was emphasized in significantly improving the catalytic performance. The presence of Sc_2O_3 on the SiO_2 support is crucial for promoting the aldol condensation of AA and the subsequent hydrogen transfer in the MPV reaction as well as triggering the dehydration of crotyl alcohol to crotonaldehyde.

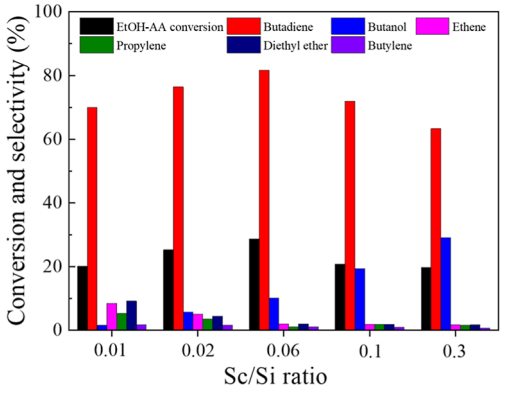

Figure 2. Influence of the Sc/Si ratio on catalytic activity. Conditions: 0.6 g of Sc_2O_3−SiO_2 catalysts at a reaction temperature of 330 °C under atmospheric pressure using EtOH-AA (75:25 wt %) as a feedstock, WHSV = 0.47 (g g^{-1} h^{-1}).

3.2. Influence of Reaction Temperature on Catalytic Activity. The influence of the reaction temperature on catalytic activity is presented in Figure 3 and Table 2. EtOH-AA conversion is controlled over the range of 20% to 30% by adjusting the WHSV. A raised reaction temperature results in an enhancement in both ethylene selectivity and diethyl ether selectivity along with a decreased selectivity of butanol. In addition, the formation of ethyl acetate with a selectivity of 6.1% is observed at a lower reaction temperature of 300 °C, which results in a low carbon balance. The selectivity of butadiene increases with the reaction temperature rising from 300 to 330 °C and decreases upon the reaction temperature rising to 380 °C. Thus, the optimized reaction temperature is 330 °C, which provides the highest butadiene selectivity.

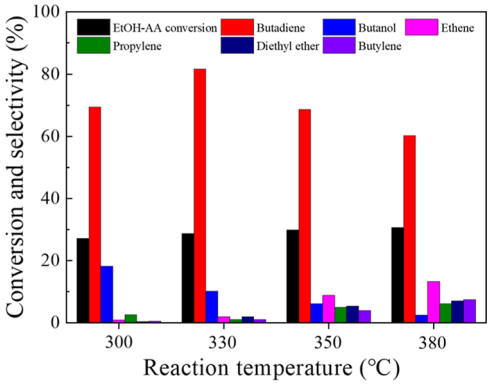

Figure 3. Influence of reaction temperature on catalytic activity. Conditions: 0.6 g of Sc_2O_3−SiO_2 (0.6) materials at a reaction temperature of 330 °C under atmospheric pressure using EtOH-AA (75:25 wt %) as a feedstock, WHSV = 0.47 (g g^{-1} h^{-1}).

3.3. Influence of WHSV on Catalytic Activity. The influence of WHSV on catalytic activity was also investigated, as presented in Figure 4 and Table 3. As WHSV increases from 0.24 g g^{-1} h^{-1} to 0.64 g g^{-1} h^{-1}, the EtOH-AA conversion decreases steadily (from 44.6% to 22.6%). There is a clear negative correlation between WHSV and the EtOH-AA conversion because a higher WHSV results in a shorter residence time of reactants on the catalyst surface. By reducing WHSV, the EtOH-AA conversion increases from 22.6% to 41.2%, resulting in a gradual increase in butadiene selectivity from 77.9% to 81.7%. However, when the EtOH-AA conversion exceeds 41.2%, the formations of byproducts such

Table 1. Influence of Sc/Si Ratio on Catalytic Activity[a]

		selectivity (%)							
Sc/Si ratio	EtOH-AA conversion (%)	butadiene	butanol	ethylene	propylene	diethyl ether	butylene	butadiene yield (%)	carbon balance (%)
0.01	20.1	69.9	1.6	8.5	5.3	9.2	1.7	14.0	96.2
0.02	25.3	76.4	5.7	5.1	3.6	4.5	1.6	19.3	96.9
0.06	28.7	81.7	10.1	2.0	1.1	2.0	1.1	23.4	98.0
0.1	20.8	71.9	19.4	1.9	1.9	1.8	1.0	15.0	97.9
0.3	19.8	63.3	29.1	1.7	1.6	1.7	0.7	12.5	98.1

[a]Conditions: 0.6 g of Sc_2O_3−SiO_2 catalysts calcined at 500 °C with a reaction temperature of 330 °C under atmospheric pressure with EtOH-AA (75:25 wt %) as a feedstock, WHSV = 0.47 (g g^{-1} h^{-1}).

https://doi.org/10.1021/acsomega.4c10129
ACS Omega 2025, 10, 7069−7076

Table 2. Influence of Reaction Temperature on Catalytic Activity[a]

reaction temperature (%)	WHSV (g g^{-1} h^{-1})	EtOH-AA conversion (%)	selectivity (%)						butadiene yield (%)	carbon balance (%)
			butadiene	butanol	ethylene	propylene	diethyl ether	butylene		
300	0.40	27.1	69.5	18.2	1.0	2.6	0.4	0.6	18.8	92.3
330	0.47	28.7	81.7	10.1	2.0	1.1	2.0	1.1	23.4	98.0
350	0.55	29.9	68.7	6.1	8.8	5.0	5.3	3.9	20.5	97.8
380	0.71	30.7	60.3	2.5	13.3	6.1	7.0	7.5	18.5	96.7

[a]Conditions: 0.5 g of Sc_2O_3−SiO_2 (0.6) catalysts calcined at 500 °C under atmospheric pressure with Sc/Si ratio of 0.06 with EtOH-AA (75:25 wt %) as a feedstock.

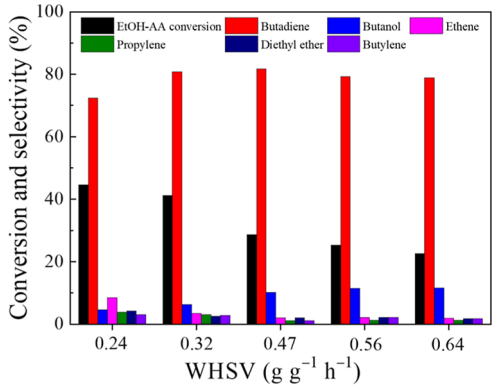

Figure 4. Influence of reaction pressure on catalytic activity. Conditions: 0.6 g of Sc_2O_3−SiO_2 (0.6) catalysts calcined at 500 °C with a reaction temperature of 330 °C under atmospheric pressure with EtOH-AA (75:25 wt %) as a feedstock.

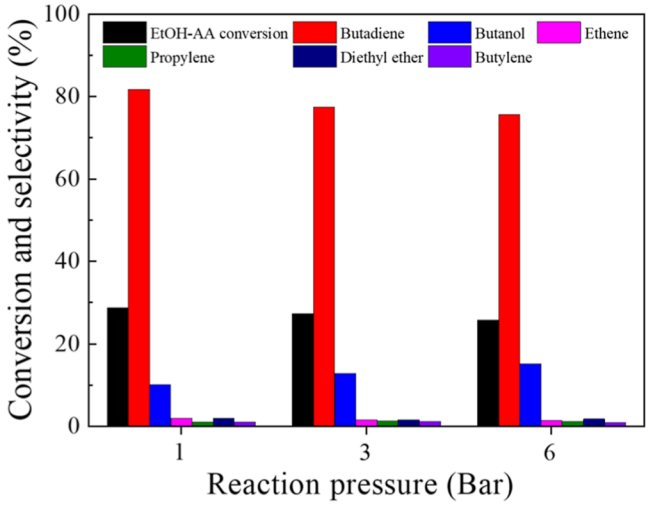

Figure 5. Influence of reaction pressure on catalytic activity. Conditions: 0.6 g of Sc_2O_3−SiO_2 (0.6) catalysts calcined at 500 °C with a reaction temperature of 330 °C with EtOH-AA (75:25 wt %) as a feedstock, WHSV = 0.47 (g g^{-1} h^{-1}).

as ethylene, propylene, and diethyl ether increase significantly, which in turn reduces butadiene selectivity. This observation indicates that the optimal conditions rely on achieving a delicate balance between high EtOH-AA conversion and high butadiene selectivity. The highest butadiene yield of 33.3% is achieved at an EtOH-AA conversion of 41.2% and a butadiene selectivity of 80.8%, corresponding to a WHSV of 0.32 g g^{-1} h^{-1}.

3.4. Influence of Reaction Pressure on Catalytic Activity. Figure 5 and Table 4 illustrate the influence of the reaction pressure on the catalytic activity. As the reaction pressure increases from 1 to 6 bar, the EtOH-AA conversion decreases gradually from 28.7% to 25.8%. This change also significantly alters the product distribution. Higher pressures promote the formation of butanol, while reducing butadiene production. The selectivity for minor products, including ethylene, propylene, diethyl ether, and butylene, remains relatively stable, with only slight variations.

3.5. N_2 Adsorption−Desorption. Figure 6 presents N_2 adsorption−desorption isotherms and BJH pore size distribution curves for the Sc_2O_3−SiO_2 catalysts with varying Sc_2O_3 content. The isotherms resemble type IV adsorption isotherms (IUPAC classification) with a hysteresis loop at higher relative pressures ($P/P_0 \approx 0.6$−0.9), indicating the characteristics of mesopores. All samples exhibit mesopores with pore diameters centered at around 12−20 nm. Higher Sc_2O_3 content results in decreased adsorption capacity and pore diameter. The surface area and pore structure of the Sc_2O_3−SiO_2 materials are summarized in Table 5. Notably, fumed silica demonstrates the highest BET surface area (340.9 m^2 g^{-1}) and pore volume (0.95 cm^3 g^{-1}). As the Sc/Si ratio increases, both the surface area and the pore volume of the Sc_2O_3−SiO_2 materials decline.

Table 3. Influence of WHSV on Catalytic Activity[a]

WHSV (g g^{-1} h^{-1})	EtOH-AA conversion (%)	selectivity (%)						butadiene yield (%)	carbon balance (%)
		butadiene	butanol	ethylene	propylene	diethyl ether	butylene		
0.24	44.6	72.4	4.6	8.5	3.8	4.2	3.1	32.3	96.6
0.32	41.2	80.8	6.3	3.4	3.1	2.5	2.8	33.3	98.9
0.47	28.7	81.7	10.1	2.0	1.1	2.0	1.1	23.4	98.0
0.56	25.3	79.3	11.5	2.1	1.3	2.2	2.1	20.1	98.5
0.64	22.6	78.9	11.6	1.9	1.2	1.8	1.8	17.8	97.2

[a]Conditions: 0.6 g of Sc_2O_3−SiO_2 (0.6) catalysts calcined at 500 °C with a reaction temperature of 330 °C under atmospheric pressure with EtOH-AA (75:25 wt %) as a feedstock.

https://doi.org/10.1021/acsomega.4c10129
ACS Omega 2025, 10, 7069−7076

Table 4. Influence of Reaction Pressure on Catalytic Activity[a]

reaction pressure (bar)	EtOH-AA conversion (%)	selectivity (%)						butadiene yield (%)	carbon balance (%)
		butadiene	butanol	ethylene	propylene	diethyl ether	butylene		
1	28.7	81.7	10.1	2.0	1.1	2.0	1.1	23.4	98.0
3	27.4	77.5	12.9	1.6	1.3	1.6	1.2	21.2	96.1
6	25.8	75.6	15.2	1.5	1.2	1.8	0.9	19.5	96.2

[a]Conditions: 0.6 g of Sc_2O_3−SiO_2 (0.6) catalysts calcined at 500 °C with a reaction temperature of 330 °C with EtOH-AA (75:25 wt %) as a feedstock, WHSV = 0.47 (g g^{-1} h^{-1}).

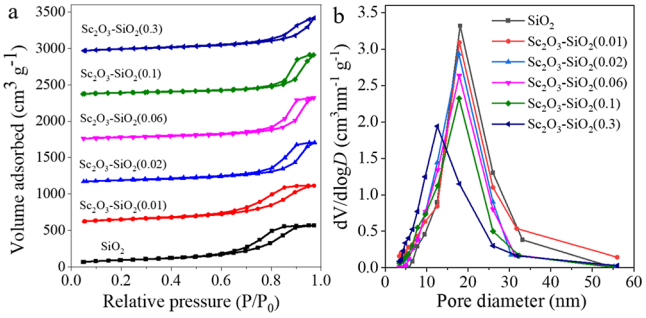

Figure 6. (a) N_2 adsorption−desorption isotherms and (b) BJH pore size distributions of the SiO_2 and Sc_2O_3−SiO_2 materials.

Table 5. Surface Area and Total Pore Volume of the Sc_2O_3−SiO_2 Samples

catalysts	total surface area (m^2 g^{-1})	average pore diameter (nm)	total pore volume (cm^3 g^{-1})
SiO_2	340.9	18.1	0.95
Sc_2O_3−SiO_2 (0.01)	336.8	17.9	0.93
Sc_2O_3−SiO_2 (0.02)	288.9	17.7	0.91
Sc_2O_3−SiO_2 (0.06)	257.5	17.6	0.89
Sc_2O_3−SiO_2 (0.1)	216.3	17.4	0.86
Sc_2O_3−SiO_2 (0.3)	193.2	12.6	0.79

The reduction is likely due to Sc_2O_3 partially obstructing the surface pores of the silica support.

3.6. X-ray Diffraction. SiO_2, Sc_2O_3, and Sc_2O_3−SiO_2 materials with different Sc/Si ratios were analyzed by the XRD technique, which was employed to detect the structural information on these catalysts. The result is exhibited in Figure 7. A wide band at 20° is attributed to amorphous SiO_2. No peaks belonging to Sc_2O_3 are observed for the Sc_2O_3−SiO_2 materials with Sc/Si ratios of less than 0.1, indicating that the Sc_2O_3 has a high dispersion. With further increasing of Sc/Si ratio to 0.3, the formation of crystalline Sc_2O_3 was demonstrated due to the presence of sharp peaks at 31.4°, 52.5°, and 62.5° ascribed to Sc_2O_3 (JCPDS42-1463).[31]

3.7. NH_3-TPD and CO_2-TPD. NH_3-TPD and CO_2TPD were employed to characterize the properties of the acid and base sites, respectively. The results are shown in Figure 8.

No NH_3 desorption peak can be observed in the fumed silica, which indicates that the acidic sites of Sc_2O_3−SiO_2 catalysts originate from the addition of Sc. In order to further investigate the density and strength of the acidic sites, the NH_3−TPD bands were divided into three peaks: weak acid sites (180 °C), medium acid sites (235 °C), and strong acid sites (325 °C), as shown in Figure 8a. Distribution and density

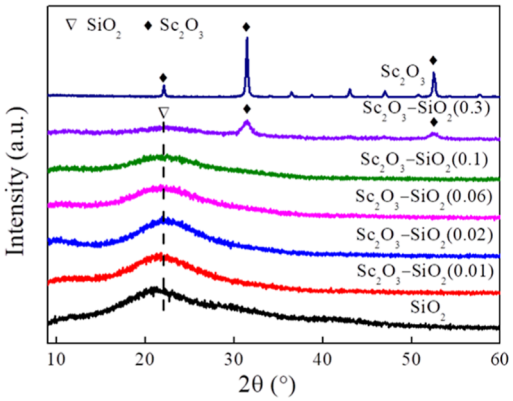

Figure 7. XRD patterns of the SiO_2, Sc_2O_3, and Sc_2O_3−SiO_2 materials.

of acidic sites were analyzed and are presented in Table 6. An increased Sc/Si ratio leads to increased densities in weak and total acid sites. The density in medium and strong acid sites rises with the Sc/Si ratio rising from 0.01 to 0.1 and declines upon further rising to 0.3. The proportion of strong acid sites in total acid sites exhibits a volcanic curve and has the highest value at a Sc/Si ratio of 0.06.

The CO_2-TPD bands were also deconvoluted to three desorption peaks: weak basic sites (200 °C), medium basic sites (285 °C), and strong basic sites (345 °C). The results are presented in Figure 8b and Table 7. Density of total base sites increases first and then decreases with the Sc/Si ratio increasing, obtaining the highest value at a Sc/Si ratio of 0.02. Density of strong base sites continuously rises with the Sc/Si ratio increase from 0.01 to 0.3. Especially, as the Sc/Si ratios increase to 0.1 and 0.3, the Sc_2O_3−SiO_2 catalysts are dominated by strong base sites.

SiO_2, as a neutral support material, typically does not possess a significant density of acidic or basic sites. While surface hydroxyl groups are present on silica, they are relatively weak and do not exhibit strong acidic or basic properties. This is in contrast to materials such as Sc_2O_3, which can introduce both acidic and basic sites when incorporated into the silica matrix. The Sc_2O_3−SiO_2 catalyst shows enhanced acidic and basic site densities due to the presence of Sc_2O_3, which modifies the surface properties of the silica support.

3.8. Effect of Catalyst Acid−Base Property on Catalytic Activity. Results from the catalytic performance reveal that an optimal Sc/Si ratio of 0.06 provides the best EtOH-AA conversion (25.8%) and butadiene selectivity (81.7%). An increased Sc/Si ratio led to decreased selectivities of ethane and diethyl ether and an increased selectivity of butanol. Combined with results from the acid−base property, it is observed that acid and base properties are closely related

https://doi.org/10.1021/acsomega.4c10129
ACS Omega 2025, 10, 7069−7076

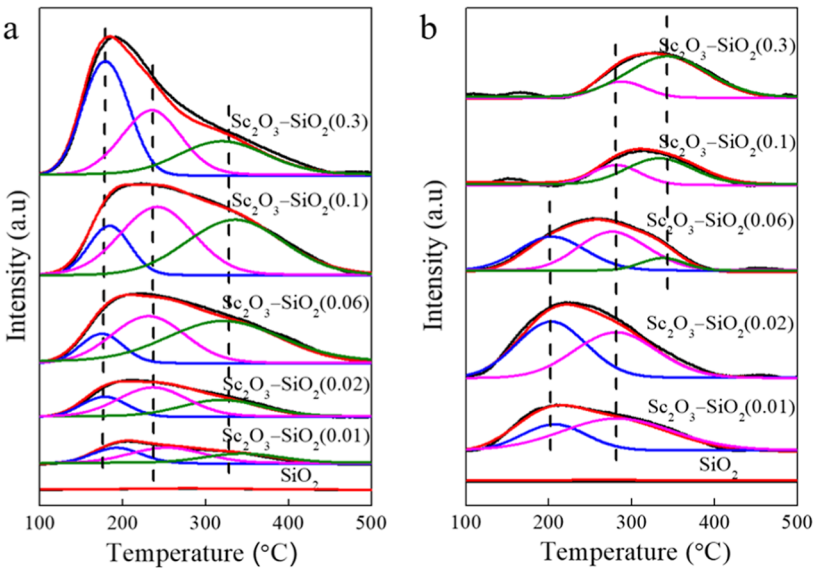

Figure 8. (a) NH_3-TPD patterns and (b) CO_2-TPD patterns for the Sc_2O_3−SiO_2 materials.

Table 6. Strength and Density of Acid Sites for the Sc_2O_3−SiO_2 Materials

	density of acidic sites (μmol g^{-1})				
catalysts	weak (80 °C)	medium (235 °C)	strong (325 °C)	total density (μmol g^{-1})	percentage of strong acid sites (%)
Sc_2O_3−SiO_2 (0.01)	8.0	11.8	7.7	27.2	28
Sc_2O_3−SiO_2 (0.02)	10.5	20.9	15.2	46.6	33
Sc_2O_3−SiO_2 (0.06)	11.0	31.3	40.1	82.4	49
Sc_2O_3−SiO_2 (0.1)	21.3	43.4	51.7	116.4	44
Sc_2O_3−SiO_2 (0.3)	57.2	43.0	32.1	132.2	24

Table 7. Strength and Density of Base Sites for the Sc_2O_3−SiO_2 Materials

	density of basic sites (μmol g^{-1})			
catalysts	weak (200 °C)	medium (285 °C)	strong (345 °C)	total density (μmol g^{-1})
Sc_2O_3−SiO_2 (0.01)	5.0	8.0	0.0	13.0
Sc_2O_3−SiO_2 (0.02)	10.6	10.9	0.0	20.5
Sc_2O_3−SiO_2 (0.06)	8.2	9.4	2.0	19.6
Sc_2O_3−SiO_2 (0.1)	0.0	2.2	7.0	9.2
Sc_2O_3−SiO_2 (0.3)	0.0	2.4	12.2	14.6

to the butadiene formation and butanol formation, respectively.

The relationship between acid−base property and activity is illustrated in Figure 9. The formations of butadiene, ethane, and diethyl ether are not directly relevant with total acid density because the increase of total acid density does not cause an increased formation of these products. The formation of butadiene is affected by both the strength and density of acid sites, as exhibited in Figure 9a. The Sc_2O_3−SiO_2 material, which has the greatest percentage of strong acid sites among the total acid sites, achieves the highest conversion of EtOH-AA and the best selectivity for butadiene, thus giving the highest butadiene yield. Different kinds of acid sites are originated from the different coordination between Sc and the

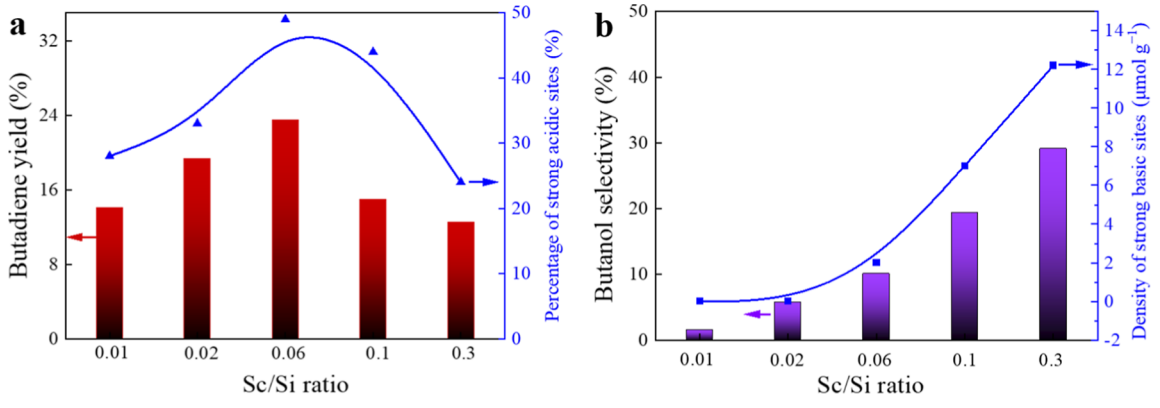

Figure 9. Relationship of (a) butadiene yield and acid property and (b) butanol selectivity and base property.

https://doi.org/10.1021/acsomega.4c10129
ACS Omega 2025, 10, 7069−7076

support. It indicates that an appropriate coordination between Sc and the support contributes to a butadiene formation and enhances butadiene selectivity.

The high butanol selectivity even up to 30% was observed. It was reported that the upgrade of EtOH to butanol is catalyzed by base sites.[32,33] In this work, as presented in Figure 9b, the production of butanol is linked to both the density and strength of the base sites. Selectivity for butanol is positively associated with the density of strong base sites, rather than the overall density of base sites. This indicates that strong base sites play a key role in catalyzing butanol formation. The strong base sites originate from the low dispersion of Sc_2O_3, as presented by the XRD result. The Sc_2O_3−SiO_2 catalysts with high Sc/Si ratios are dominated by crystal Sc_2O_3 species, as demonstrated by the XRD patterns. It can be deduced that the strong base sites originated from the lattice oxygen from crystal Sc_2O_3 species.

Weak acid and weak base sites, however, are less effective in driving these specific reactions and tend to lead to the formation of side products such as ethene and diethyl ether. As a result, the presence of weak acid and base sites can lower the selectivity for butadiene and butanol. Summarily, the distribution and strength of acid−base sites in the catalyst directly influence the selectivity toward different products, with high-intensity acid−base sites promoting butadiene or butanol formation and weaker sites leading to the formation of undesired byproducts.

4. CONCLUSIONS

In conclusion, the Sc_2O_3−SiO_2 material with a Sc/Si ratio of 0.06 has demonstrated remarkable efficacy in the upgrade of EtOH-AA to butadiene, achieving a selectivity of 81.7% at 330 °C. The success of this catalyst can be attributed to its unique structural and acidic−basic properties. The presence of a higher proportion of strong acid sites facilitates the formation of butadiene, while the increased density of strong basic sites promotes the production of butanol.

■ ASSOCIATED CONTENT

Supporting Information

The Supporting Information is available free of charge at https://pubs.acs.org/doi/10.1021/acsomega.4c10129.

Photograph of the setup for the conversion of ethanol to butadiene (PDF)

■ AUTHOR INFORMATION

Corresponding Author

Bin Wang − *National Energy R&D Center for Biorefinery, Beijing University of Chemical Technology, Beijing 100029, P. R. China; Beijing Key Laboratory of Bioprocess, Beijing University of Chemical Technology, Beijing 100029, P. R. China;* orcid.org/0000-0002-5578-6747; Email: wangbin@mail.buct.edu.cn

Authors

Qiangqiang Zhu − *National Energy R&D Center for Biorefinery, Beijing University of Chemical Technology, Beijing 100029, P. R. China; Department of Hydrogenation Catalyst, Sinopec Research Institute of Petroleum Processing, Beijing 100083, PR China;* orcid.org/0000-0002-8393-6589

Lilin Yin − *National Energy R&D Center for Biorefinery, Beijing University of Chemical Technology, Beijing 100029, P. R. China*

Xianyao Han − *Beijing Key Laboratory of Bioprocess, Beijing University of Chemical Technology, Beijing 100029, P. R. China*

Complete contact information is available at: https://pubs.acs.org/10.1021/acsomega.4c10129

Notes

The authors declare no competing financial interest.

■ ACKNOWLEDGMENTS

We gratefully acknowledge the support of the National Key Research and Development Program of China (2022YFC2104701), the Project from SINOPEC (224200), and the Major Science and Technology Achievement Transformation Project of the Hebei Provincial Department of Science and Technology (23262802Z).

■ REFERENCES

(1) Wang, C.; Huo, S.; Ye, G.; Wang, B.; Guo, Z.; Zhang, Q.; Song, P.; Wang, H.; Liu, Z. Construction of an Epoxidized, Phosphorus-Based Poly (Styrene Butadiene Styrene) and Its Application in High-Performance Epoxy Resin. *Composites, Part B* **2024**, *268*, 111075.

(2) Ge, S.; Ouyang, H.; Ye, H.; Shi, Y.; Sheng, Y.; Peng, W. High-Performance and Environmentally Friendly Acrylonitrile Butadiene Styrene/Wood Composite for Versatile Applications in Furniture and Construction. *Adv. Compos. Hybrid Mater.* **2023**, *6* (1), 44.

(3) Singh, P.; Katiyar, P.; Singh, H. Impact of Compatibilization on Polypropylene (PP) and Acrylonitrile Butadiene Styrene (ABS) Blend: A Review. *Mater. Today Proc.* **2023**, *78*, 189−197.

(4) Yang, J.; Wang, P.; Neumann, H.; Jackstell, R.; Beller, M. Industrially Applied and Relevant Transformations of 1,3-Butadiene Using Homogeneous Catalysts. *Ind. Chem. Mater.* **2023**, *1* (2), 155−174.

(5) Zhang, L.; Pham, T. N.; Faria, J.; Resasco, D. E. Improving the Selectivity to C4 Products in the Aldol Condensation of Acetaldehyde in Ethanol over Faujasite Zeolites. *Appl. Catal. Gen.* **2015**, *504*, 119−129.

(6) Bruijnincx, P. C. A.; Weckhuysen, B. M. Shale Gas Revolution: An Opportunity for the Production of Biobased Chemicals? *Angew. Chem., Int. Ed.* **2013**, *52* (46), 11980−11987.

(7) Chung, S.-H.; Li, T.; Shoinkhorova, T.; Komaty, S.; Ramirez, A.; Mukhambetov, I.; Abou-Hamad, E.; Shterk, G.; Telalovic, S.; Dikhtiarenko, A.; Sirks, B.; Lavrik, P.; Tang, X.; Weckhuysen, B. M.; Bruijnincx, P. C. A.; Gascon, J.; Ruiz-Martínez, J. Origin of Active Sites on Silica−Magnesia Catalysts and Control of Reactive Environment in the One-Step Ethanol-to-Butadiene Process. *Nat. Catal.* **2023**, *6* (4), 363−376.

(8) Wang, K.; Chen, C.; Gao, W.; Liu, N.; Wang, C.; Wang, F.; Fan, J.; Gu, Y.; Zhu, C.; Tsubaki, N. Green and Rapid Synthesis of Hierarchical Nano-Sized Pure Si-Beta Zeolite Supported with Zn and Y for Effective Synthesis of Butadiene from Aqueous Ethanol. *Chem. Eng. J.* **2024**, *479*, 147780.

(9) Chung, S.; de Miguel, J. C. N.; Li, T.; Lavrik, P.; Komaty, S.; Yuan, Y.; Poloneeva, D.; Anbari, W. H.; Hedhili, M. N.; Zaarour, M.; Martín, C.; Shoinkhorova, T.; Abou−Hamad, E.; Gascon, J.; Ruiz−Martínez, J. Core−Shell Structured Magnesia−Silica as a next Generation Catalyst for One-Step Ethanol-to-Butadiene Lebedev Process. *Appl. Catal., B* **2024**, *344*, 123628.

(10) Zhu, Q.; Wang, B.; Tan, T. Conversion of Ethanol and Acetaldehyde to Butadiene over MgO−SiO_2 Catalysts: Effect of Reaction Parameters and Interaction between MgO and SiO_2 on Catalytic Performance. *ACS Sustain. Chem. Eng.* **2017**, *5* (1), 722−733.

(11) Szabó, B.; Hutkai, V.; Novodárszki, G.; Lónyi, F.; Pászti, Z.; Fogarassy, Z.; Valyon, J.; Barthos, R. A Study of the Conversion of Ethanol to 1,3-Butadiene: Effects of Chemical and Structural Heterogeneity on the Activity of $MgO-SiO_2$ Mixed Oxide Catalysts. *React. Chem. Eng.* **2023**, *8* (3), 718−731.
(12) Samsudin, I. B.; Jaenicke, S.; Chuah, G.-K. Conversion of Ethanol to Butadiene over Binary $MgO-SiO_2$ Mixed Oxides Prepared by the Ammonia Evaporation Method. *Chemistry* **2023**, *5* (1), 544−558.
(13) Li, X.; Zhao, Y.; Pang, J.; Wu, P.; Yu, W.; Yan, P.; Su, Y.; Zhai, S.; Zheng, M. Cu-Zr/SiO_2 Catalysts Featured by Different Cu-Zr-Si Coordinations for Ethanol Conversion to 1,3-Butadiene. *Resour. Chem. Mater.* **2024**, *3* (1), 27−37.
(14) Akhade, S. A.; Winkelman, A.; Lebarbier Dagle, V.; Kovarik, L.; Yuk, S. F.; Lee, M.-S.; Zhang, J.; Padmaperuma, A. B.; Dagle, R. A.; Glezakou, V.-A.; Wang, Y.; Rousseau, R. Influence of Ag Metal Dispersion on the Thermal Conversion of Ethanol to Butadiene over Ag-ZrO_2/SiO_2 Catalysts. *J. Catal.* **2020**, *386*, 30−38.
(15) Li, H.; Pang, J.; Jaegers, N. R.; Kovarik, L.; Engelhard, M.; Savoy, A. W.; Hu, J.; Sun, J.; Wang, Y. Conversion of Ethanol to 1,3−Butadiene over Ag−ZrO_2/SiO_2 Catalysts: The Role of Surface Interfaces. *J. Energy Chem.* **2021**, *54*, 7−15.
(16) Liu, C.; Li, Y.; Wu, L.; Geng, Z. Synthesis of 1,3-Butadiene from Ethanol/Acetaldehyde over ZrO_2-MgO-SiO_2 Catalyst: The Thermodynamics and Reaction Kinetics Analysis. *Chem. Eng. J.* **2021**, *421*, 127861.
(17) Cabello González, G. M.; Villanueva Perales, A. L.; Campoy, M.; López Beltran, J. R.; Martínez, A.; Vidal-Barrero, F. Kinetic Modelling of the One-Step Conversion of Aqueous Ethanol into 1,3-Butadiene over a Mixed Hemimorphite-HfO_2/SiO_2 Catalyst. *Fuel Process. Technol.* **2021**, *216*, 106767.
(18) Wang, C.; Zheng, M.; Li, X.; Li, X.; Zhang, T. Catalytic Conversion of Ethanol into Butadiene over High Performance LiZnHf-MFI Zeolite Nanosheets. *Green Chem.* **2019**, *21* (5), 1006−1010.
(19) De Baerdemaeker, T.; Feyen, M.; Müller, U.; Yilmaz, B.; Xiao, F.-S.; Zhang, W.; Yokoi, T.; Bao, X.; Gies, H.; De Vos, D. E. Bimetallic Zn and Hf on Silica Catalysts for the Conversion of Ethanol to 1,3-Butadiene. *ACS Catal.* **2015**, *5* (6), 3393−3397.
(20) Qi, L.; Zhang, Y.; Conrad, M. A.; Russell, C. K.; Miller, J.; Bell, A. T. Ethanol Conversion to Butadiene over Isolated Zinc and Yttrium Sites Grafted onto Dealuminated Beta Zeolite. *J. Am. Chem. Soc.* **2020**, *142* (34), 14674−14687.
(21) Yan, T.; Dai, W.; Wu, G.; Lang, S.; Hunger, M.; Guan, N.; Li, L. Mechanistic Insights into One-Step Catalytic Conversion of Ethanol to Butadiene over Bifunctional Zn−Y/Beta Zeolite. *ACS Catal.* **2018**, *8* (4), 2760−2773.
(22) Dochain, D. D.; Styskalik, A.; Vykoukal, V.; Vimont, A.; Travert, A.; Debecker, D. P. Non-Hydrolytic Sol−Gel Routes to Bifunctional Cu−Ta−SiO_2 Catalysts for the Upgrading of Ethanol to Butadiene. *Chem. Mater.* **2023**, *35* (17), 7113−7124.
(23) Mamedov, K.; Davis, R. J. Cascade Reaction of Ethanol to Butadiene over Ag-Promoted, Silica- or Zeolite-Supported Ta, Y, Pr, or La Oxide Catalysts. *ACS Catal.* **2023**, *13* (5), 3333−3344.
(24) Cabello González, G. M.; Villanueva Perales, A. L.; Martínez, A.; Campoy, M.; Vidal-Barrero, F. Conversion of Aqueous Ethanol/Acetaldehyde Mixtures into 1,3-Butadiene over a Mesostructured Ta-SBA-15 Catalyst: Effect of Reaction Conditions and Kinetic Modelling. *Fuel Process. Technol.* **2022**, *226*, 107092.
(25) Wang, K.; Gao, W.; Chen, F.; Liu, G.; Wu, J.; Liu, N.; Kawabata, Y.; Guo, X.; He, Y.; Zhang, P.; Yang, G.; Tsubaki, N. Hierarchical Nano-Sized ZnZr-Silicalite-1 Multifunctional Catalyst for Selective Conversion of Ethanol to Butadiene. *Appl. Catal., B* **2022**, *301*, 120822.
(26) Cabello González, G. M.; Villanueva Perales, A. L.; Campoy, M.; López Beltran, J. R.; Martínez, A.; Vidal-Barrero, F. Kinetic Modelling of the One-Step Conversion of Aqueous Ethanol into 1,3-Butadiene over a Mixed Hemimorphite-HfO_2/SiO_2 Catalyst. *Fuel Process. Technol.* **2021**, *216*, 106767.
(27) Yang, G.; Wang, L.; Jiang, H. Preparation of β Zeolite with Intracrystalline Mesoporosity via Surfactant-Templating Strategy and Its Application in Ethanol-Acetaldehyde to Butadiene. *Microporous Mesoporous Mater.* **2021**, *316*, 110949.
(28) Kyriienko, P. I.; Larina, O. V.; Soloviev, S. O.; Orlyk, S. M.; Dzwigaj, S. High Selectivity of TaSiBEA Zeolite Catalysts in 1,3-Butadiene Production from Ethanol and Acetaldehyde Mixture. *Catal. Commun.* **2016**, *77*, 123−126.
(29) Zhu, Q.; Yin, L.; Ji, K.; Li, C.; Wang, B.; Tan, T. Effect of Catalyst Structure and Acid−Base Property on the Multiproduct Upgrade of Ethanol and Acetaldehyde to C_4 (Butadiene and Butanol) over the Y−SiO_2 Catalysts. *ACS Sustain. Chem. Eng.* **2020**, *8*, 1555.
(30) Zhang, H.; Tan, H.-R.; Jaenicke, S.; Chuah, G.-K. Highly Efficient and Robust Cu Catalyst for Non-Oxidative Dehydrogenation of Ethanol to Acetaldehyde and Hydrogen. *J. Catal.* **2020**, *389*, 19−28.
(31) Li, J.-G.; Ikegami, T.; Mori, T.; Yajima, Y. Sc_2O_3 Nanopowders via Hydroxyl Precipitation: Effects of Sulfate Ions on Powder Properties. *J. Am. Ceram. Soc.* **2004**, *87* (6), 1008−1013.
(32) Chakraborty, S.; Piszel, P. E.; Hayes, C. E.; Baker, R. T.; Jones, W. D. Highly Selective Formation of *n*-Butanol from Ethanol through the Guerbet Process: A Tandem Catalytic Approach. *J. Am. Chem. Soc.* **2015**, *137* (45), 14264−14267.
(33) Chieregato, A.; Velasquez Ochoa, J.; Bandinelli, C.; Fornasari, G.; Cavani, F.; Mella, M. On the Chemistry of Ethanol on Basic Oxides: Revising Mechanisms and Intermediates in the Lebedev and Guerbet Reactions. *ChemSusChem* **2015**, *8* (2), 377−388.

https://doi.org/10.1021/acsomega.4c10129
ACS Omega 2025, 10, 7069−7076